Hyperspectral Imaging of Nanoparticles in Biological Samples: Simultaneous Visualization and Elemental Identification

MARÍA DEL PILAR SOSA PEÑA,[1] ABHISHEK GOTTIPATI,[1] SAHIL TAHILIANI,[1] NICOLE M. NEU-BAKER,[1] MARY D. FRAME,[2] ADAM J. FRIEDMAN,[3] AND SARA A. BRENNER[1]*

[1]*College of Nanoscale Science, Nanobioscience Constellation, State University of New York (SUNY) Polytechnic Institute, Albany, New York 12203*

[2]*Department of Biomedical Engineering, State University of New York (SUNY) Stony Brook, Stony Brook, New York 11794*

[3]*George Washington School of Medicine and Health Sciences, Department of Dermatology, Washington, District of Columbia 20037*

KEY WORDS aluminum oxide; cerium oxide; dark-field microscopy; engineered nanomaterials

ABSTRACT While engineered nanomaterials (ENMs) are increasingly incorporated into industrial processes and consumer products, the potential biological effects and health outcomes of exposure remain unknown. Novel advanced direct visualization techniques that require less time, cost, and resource investment than electron microscopy (EM) are needed for identifying and locating ENMs in biological samples. Hyperspectral imaging (HSI) combines spectrophotometry and imaging, using advanced optics and algorithms to capture a spectrum from 400 to 1000 nm at each pixel in an enhanced dark-field microscopic (EDFM) image. HSI-EDFM can be used to confirm the identity of the materials of interest in a sample and generate an image "mapping" their presence and location in a sample. Hyperspectral mapping is particularly important for biological samples, where ENM morphology is visually indistinct from surrounding tissue structures. While use of HSI (without mapping) is increasing, no studies to date have compared results from hyperspectral mapping with conventional methods. Thus, the objective of this study was to utilize EDFM-HSI to locate, identify, and map metal oxide ENMs in *ex vivo* histological porcine skin tissues, a toxicological model of cutaneous exposure, and compare findings with those of Raman spectroscopy (RS), energy-dispersive X-ray spectroscopy (EDS), and scanning electron microscopy (SEM). Results demonstrate that EDFM-HSI mapping is capable of locating and identifying ENMs in tissue, as confirmed by conventional methods. This study serves as initial confirmation of EDFM-HSI mapping as a novel and higher throughput technique for ENM identification in biological samples, and serves as the basis for further protocol development utilizing EDFM-HSI for semiquantitation of ENMs. *Microsc. Res. Tech. 79:349–358, 2016.*

INTRODUCTION

Engineered nanomaterials (ENMs) are increasingly incorporated into manufacturing processes and products in a variety of industries. Meanwhile, the nanotechnology workforce is also growing: 2 million nanotechnology workers are projected to work in the US by 2020, part of a global nanotechnology workforce of 6 million (Roco et al., 2010). Currently, the physiological effects and potential health impacts of occupational exposures to ENMs are not fully understood.

The semiconductor industry utilizes ENMs in silicon wafer fabrication during wafer polishing processes. Two of the most common metal oxide nanoparticle abrasives used in this manner include cerium oxide (CeO_2; ceria) and aluminum oxide (Al_2O_3; alumina) (Brenner et al., 2015; Brenner and Neu-Baker, 2014; Roth et al., 2015a). Semiconductor workers who handle these ENMs may be exposed via inhalation or cutaneous contact (Brenner et al., 2015; Brenner and Neu-Baker, 2015; Shepard and Brenner, 2014a,b). While occupational exposure assessment seeks to define and quantify worker exposures, the use of complementary animal models seeks to define the toxicological profiles (hazard) of the ENMs in use. In this way, investigators

This article was published online on February 11, 2016. After online publication, an error in the color description in figure 6 was subsequently identified. This notice is included in the online and print versions to indicate that both have corrected on March 17, 2016.

*Correspondence to: Sara A. Brenner, MD, MPH, State University of New York (SUNY) Polytechnic Institute, College of Nanoscale Science, Nanobioscience Constellation, 257 Fuller Road, Albany, New York 12203, United States of America. E-mail: sbrenner@sunypoly.edu

Received 16 December 2015; accepted in revised form 21 January 2016

Abbreviations: DLS, dynamic light scattering; EDFM, enhanced darkfield microscopy; EDS, , energy-dispersive X-ray spectroscopy; ENM, engineered nanomaterial; HSI, hyperspectral imaging; ROI, region of interest; ROS, reactive oxygen species; RS, Raman spectroscopy; RSL, reference spectral library; SAM, spectral angle mapper; SEM, scanning electron microscopy; SL, spectral library; VNIR, visible and near infrared

Additional Supporting Information may be found in the online version of this article.

REVIEW EDITOR: Prof. George Perry

Contract grant sponsor: CDC-NIOSH; Contract grant number: OH-009990-01A1; Contract grant sponsor: NanoHealth and Safety Center, New York State.

DOI 10.1002/jemt.22637

Published online 11 February 2016 in Wiley Online Library (wileyonlinelibrary.com).

will be positioned to better understand and address the overall risk to workers who handle industrial ENMs (Risk = Exposure × Hazard).

As histological samples are commonly used for toxicology studies, an efficient visualization technique that allows for the detection and characterization of ENMs in a fast and an inexpensive way while preserving the tissue structure is greatly needed. Hyperspectral imaging (HSI) has emerged as a new technology for analysis of nanoscale materials that combines spectrophotometry and imaging using advanced optics and algorithms to capture spectral data in the visible and near-infrared (VNIR) wavelengths for each pixel in an enhanced dark-field microscopic (EDFM) image. Spectral profiles can be collected for known materials and used as a spectral library (SL) for comparison of materials found in other samples through a mapping process, which, although crucial to identify nonmorphologically distinct particles, is not universally used in HSI studies. EDFM allows for increased contrast, facilitating visualization of nanoscale materials in a variety of matrices (Roth et al., 2015b). Protocols for EDFM and HSI as well as potential applications for this imaging modality have previously been presented in detail by Roth et al. (2015a,b,c). While EDFM-HSI for visualization and identification of ENMs in histological tissue samples has been reported (Husain et al., 2013; Kwok et al., 2012; Ma et al., 2012; Mercer et al., 2013; Roth et al., 2015b; Vetten et al., 2013), only some have utilized the HSI spectral mapping capabilities for compositional analysis (Husain et al., 2015; Ilves et al., 2014; Roth et al., 2015b; Vetten et al., 2013) and, to the best of our knowledge, none have reported a systematic confirmation of the technique.

The identification of morphologically distinct ENMs by EDFM and/or HSI is relatively straightforward, as in the case of carbon nanotubes (CNTs). Confident identification of CNTs can be made by direct visualization with EDFM without the need for elemental confirmation by hyperspectral mapping (Mercer et al., 2013). However, other ENMs with indistinctive shapes, such as the spherical metal oxide ENMs used in this study, can either remain isolated or cluster together. These ENMs are much more difficult, if not impossible, to distinguish from native biological structures or artifacts on the basis of direct visualization alone. In these cases, confirmation of the ENM's identity requires the creation of reference SLs (RSLs) from positive and negative controls that is used for subsequent ENM mapping in experimental samples. The creation of the RSLs, which is the basis for the mapping process, requires an initial visual detection of high contrast elements in the EDFM image, which could represent not only the suspected ENMs of interest (Roth et al., 2015b), but also other objects in the tissue, such as debris and artifacts, as reported by Husain et al. (2015). Therefore, it is imperative that the RSLs created are based on spectral profiles from the true ENMs of interest (positive controls) and from samples completely free of the ENMs of interest (negative controls). Accurate RSLs are the key to sensitive and specific mapping of ENMs in experimental samples. The crucial initial step of generating an SL from a positive control is initially based on a visual detection of ENMs in the sample by the microscopist/researcher; therefore, positive identification of the element of interest by other conventional methods not only improves mapping accuracy but also provides necessary confirmation of ENM identity. Such validation of this novel EDFM-HSI approach has been achieved through comparison to traditional methods. The gold standard for ENM imaging is electron microscopy (EM)—either transmission electron microscopy (TEM) or scanning electron microscopy (SEM)—which uses a beam of accelerated electrons to create an image of a sample with nanoscale resolution. EM can be combined with energy-dispersive X-ray spectroscopy (EDS) to determine solid surface elemental composition and visualization of nanoscale materials (Zheng et al., 2011). While EM is capable of much higher magnification and has greater resolving power than light microscopy, the time-to-knowledge and cost-of-ownership of EM are also much greater. Another well-known method is Raman spectroscopy (RS), which is based on phonon-assisted inelastic scattering of incident monochromatic light. This provides information about the vibrational energy levels within a molecule, creating a sharp and characteristic shift or peak specific to the molecule, thus providing a molecular fingerprint of the sample (Edwards, 2005; Jestel, 2010). While RS is a robust technique for nanoparticle identification, it is far more time-consuming and limiting in terms of sample preparation than HSI.

In this study, we explore the utility of EDFM-HSI with spectral mapping for localization and compositional identification of ENMs in exposed histological porcine skin tissue, which serves as a toxicological model for real-world cutaneous exposures to metal oxide ENMs. Furthermore, to confirm EDFM-HSI findings, its performance is compared alongside traditional methods—RS and SEM with EDS—used for advanced nanoscale visualization.

MATERIALS AND METHODS

Metal Oxide Nanoparticle Suspensions

Commercially available metal oxide nanoparticle suspensions used for semiconductor wafer polishing were utilized in this study. These suspensions comprised ceria or alumina nanoparticles, dispersants, surfactants, and acids or bases in deionized water. The alumina and ceria ENMs are approximately 56–100 nm in diameter, according to dynamic light scattering (DLS) analysis (Roth et al., 2015d). The nanoparticle slurry suspensions have been characterized in detail and reported by Roth et al. (2015d) (see Supporting Information for characterization data).

Porcine Skin Exposure Model

Porcine skin was obtained from the dorsolateral region of 14 freshly euthanized adult male pigs through a tissue-sharing program at Stony Brook University (Stony Brook, NY). Each experimental sample was cut into 1.5 cm long × 1.5 cm wide × 0.5 cm thick specimens to ensure that epidermis, dermis and subcutaneous layers were present. A modified Franz cell chamber with a diffusional area of 0.785 cm^2 was used to expose the porcine skin to ENM suspensions of interest. Ten porcine models were divided into two experimental groups, where five models were topically exposed to

ceria and five models to alumina nanoparticles in suspension, respectively. Two porcine models were exposed to a nanoparticle-free aqueous suspension to serve as negative controls, and two porcine models were injected (200 μm depth, through the stratum corneum) with the ceria and alumina nanoparticle-containing suspensions to serve as positive controls. Each specimen was exposed to 75 μL of nanoparticle suspension for 24 h. The total exposure was 0.0623 μg for ceria and 0.0758 μg for alumina, respectively, based on the NP concentrations in the commercial slurries. The porcine skin was placed with the epidermis facing the donor compartment and the subcutaneous tissue facing the receptor compartment. The epidermal surface was exposed to the aqueous suspensions of metal oxide nanoparticles while the receptor compartment was filled with phosphate buffered saline. All exposures were performed within a chemical fume hood, with room temperature maintained at 23–25°C at 50–60% humidity.

Histological Preparation

Following exposure, skin tissues were fixed via immersion in 10% formalin and stored in the fixative until histological preparation by the Albert Einstein College of Medicine (AECOM) Histology and Comparative Pathology Facility (Bronx, NY). Briefly, fixed tissues were processed through solvents and embedded in paraffin using a Leica Tissue Processor (Leica; Wetzlar, Germany). Paraffin-embedded tissues were sectioned to a 6 μm thickness using a rotary microtome. The tissues were sectioned directionally from subcutaneous to epidermal layer, using a clean blade for each cut, as to minimize risk of artificially trafficking particles in the direction of potential penetration, and mounted onto glass microscopy slides. Deparaffinized and rehydrated tissue sections were stained with hematoxylin and eosin (H&E), and then dehydrated through graded alcohols to xylene and coverslipped (Kumar et al., 2010; Titford, 2009). For the positive control samples, the fixed tissue was sectioned to generate three serial sections: one section was H&E stained and coverslipped for dark-field and bright-field microscopy; the other two sections remained unstained and mounted onto glass microscopy slides for RS and SEM-EDS. No coverslip was applied to these samples for RS, and SEM-EDS analysis; only a layer of paraffin remained on the sample for tissue preservation until use. To remove the remaining paraffin layer from the tissue, the noncoverslipped slides were warmed at 50°C for 30 min followed by immersion in xylene for 5 min. While H&E or other histological stains are not necessary for HSI, this provided the opportunity to also examine these tissues in bright-field, where the stained tissues would be more easily visualized. Regardless of the sample preparation method, any sample for HSI must be coverslipped to protect the specimen from the objective lens, especially when using an oil immersion 100× objective lens.

Enhanced Dark-Field Microscopy (EDFM) and Hyperspectral Imaging (HSI)

A total of 14 samples (5 exposed to ceria; 5 exposed to alumina; 2 positive controls; 2 negative controls) were visualized at SUNY Polytechnic Institute (Albany, NY) with a CytoViva HSI system (Auburn, AL) mounted on an Olympus BX-43 microscope with an EDFM condenser to locate and identify ENMs. Images were obtained with a DAGE optical camera system for EDFM, and with a Pixelfly camera system for HSI that captures spectral data per pixel in the VNIR region. Consistent exposure settings were maintained for scanning and imaging purposes for all samples (for DAGE EDFM camera: gain 3.0 dB, shutter 35 ms, 75% brightness; for Pixelfly HSI camera: 720 lines, 0.25 s exposure time). Lamp correction was considered unnecessary for the samples investigated in this study as initial comparison between lamp-corrected and non-lamp-corrected datacubes produced no differences in mapping (Roth et al., 2015b; direct communication with CytoViva, Inc. on May 27–28, 2015). However, this may not be the case for other samples, which may require lamp correction. For the injected positive control samples, different areas with the highest load of ENMs were imaged by EDFM and HSI in each skin layer (epidermis, dermis, and subcutaneous tissue). EDFM was first performed to detect areas of high contrast to identify them as areas of interest. Using the HSI camera, datacubes (HSI images) were captured and analyzed for each sample using the ENVI 4.8 HSI software and following the method described by Roth et al. (2015b). Once the areas of interest were captured with HSI, the findings were confirmed with RS and SEM-EDS as described below, and then followed by the creation of a preliminary spectral library (SL), obtained from the positive control datacubes for each ENM type via the ENVI particle filter function. For the negative vehicle control samples, areas without high-contrast elements were selected for imaging and analysis. Utilizing the preliminary SL from the positive control, a reference spectral library (RSL) was generated for HSI experimental sample mapping. For the creation of each RSL, the preliminary positive control SLs were filtered against the negative control datacubes to subtract all duplicative spectra, thus increasing specificity (Roth et al., 2015b). This filtering process utilizes data from both the positive and negative controls to create the RSL, which is then used for mapping. Next, experimental samples exposed topically to ENMs in solution were imaged with EDFM. HSI datacubes from these experimental samples were captured, analyzed, and mapped against their respective RSL.

While it is known that spectral data is highly dependent on the sample matrix and microenvironment (Roth et al., 2015b), an SL was created from the raw ENMs in solution for comparison to the SLs of the injected positive control samples to determine which SL was appropriate for creation of the RSL for mapping.

HSI Mapping

Following the identification of ENMs and their capture in datacubes for each experimental sample, each datacube was mapped against its respective RSL using the ENVI spectral angle mapper (SAM) function, as specified in Roth et al. (2015b), to create an image that showed the areas where nanoparticles were present in a particular color overlaid on the original datacube. The default SAM threshold (0.10) was used for this study.

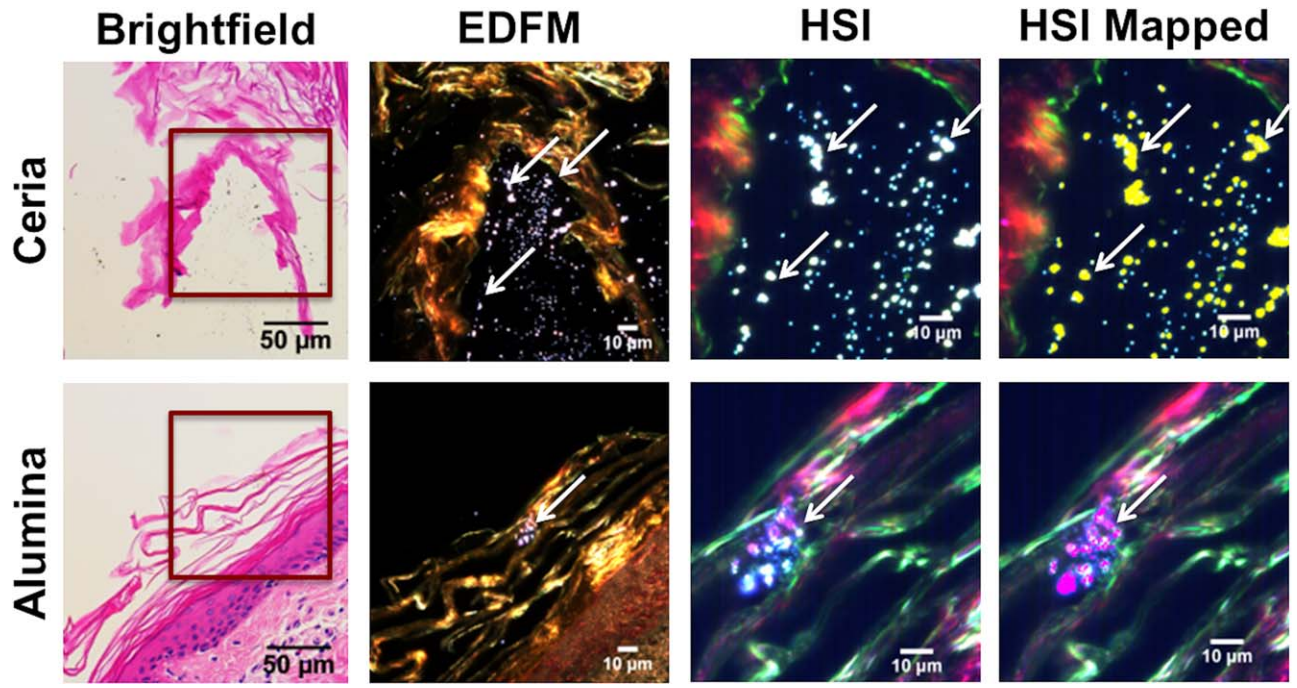

Fig. 1. Positive control porcine skin tissue viewed by bright-field microscopy, EDFM, and HSI with mapping. Rows correspond to the stratum corneum of porcine skin tissue injected with ceria and alumina nanoparticles. Each column shows the same field of view imaged with different techniques. The first column corresponds to the bright-field view of H&E stained stratum corneum (40× magnification). The area enclosed in a red square is magnified to 100× and viewed using EDFM (column 2) and HSI (column 3), where ENMs appear as high-contrast elements, indicated by arrows. Column 4 shows the HSI image mapped against the RSL, where the ENMs with positive matching are shown in yellow for ceria (arrows) and in magenta for alumina (arrows). [Color figure can be viewed in the online issue, which is available at wileyonlinelibrary.com.]

Raman Spectroscopy (RS)

An HORIBA Jobin Yvon's LabRAM 800HR Raman spectrometer was used to validate the HSI findings. The positive control samples that had been imaged with EDFM and HSI for the localization of ENMs were analyzed with RS to verify the presence of the characteristic spectral peak that is produced for each specific element. First, each of the concentrated ENM-containing solutions (ceria, alumina) was drop-cast on a silicon substrate and was characterized using a 532 nm (2.33 eV) and 633 nm laser (1.96 eV). For ceria, acquisition time was 5 s averaged 20 times at 2.25 mW laser power, using 532 nm laser. For alumina, acquisition time was 10 s averaged 10 times at 5.5 mW laser power, using 633 nm laser. Spectral peaks were recorded for further comparison. This characterization was performed in duplicate to confirm the specific peaks obtained.

The paraffin layer was removed from the positive control unstained noncoverslipped slides created from serial tissue sections for RS and SEM-EDS analysis by heating the slide on a hot plate for 30 min at 50°C followed by a 5 min immersion in 100% xylene. Using RS, areas of interest were localized, imaged at 100× magnification, and analyzed to compare their spectral peaks with the spectral peaks expected for the specific nanomaterial to which they had been exposed. The spectral peaks obtained from the concentrated ENM-containing solutions and the spectral peaks obtained from the positive control samples were analyzed and compared.

Scanning Electron Microscopy (SEM) and Energy-Dispersive X-Ray Spectroscopy (EDS)

Zeiss 1550 FE-SEM with in-lens and secondary electron detector integrated with a Bruker Quantax energy-dispersive X-ray spectrometer was used to identify the nanoparticles in the skin tissue samples. The microscopy slides with deparaffinized tissue were attached to sample pin stub mounts for SEM imaging. The images were captured using secondary electron (Everhart-Thornley) detector using acceleration voltage of 20 kV, at a working distance of 15–15.2 mm. A Bruker Quantax energy-dispersive X-ray spectrometer was used to confirm the elemental composition of nanoparticle-exposed tissue. EDS-based elemental distribution maps of the regions of interest (ROI) were obtained and overlaid on the corresponding SEM images.

RESULTS

Nanoparticle Identification with EDFM and HSI and Spectral Mapping

High-contrast elements (suspected nanoparticles) were identified in the positive control (injected tissue) samples, while they show as dark spots in the bright-field view as shown in Figure 1. Because the shape of the high-contrast elements was indistinctive, and no spectral reference library exists for comparison, the presence of the ENMs of interest was confirmed with RS (Fig. 2), and SEM-EDS (Figs. 3 and 4). Once the three methods confirmed the presence of the expected ENMs, the creation of an SL from the positive control

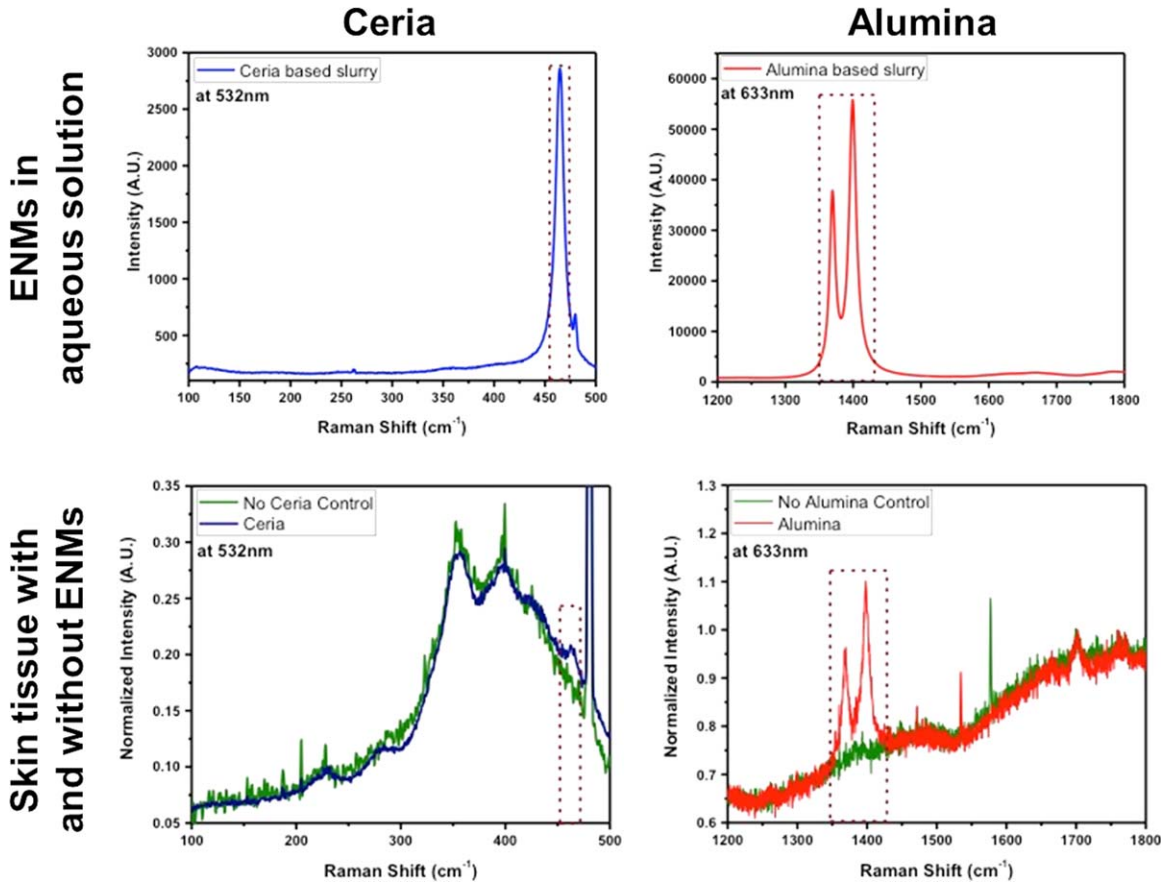

Fig. 2. Raman spectra of metal oxide nanoparticles in aqueous solution compared to metal oxide nanoparticles embedded in porcine skin tissue. A spectral profile was obtained from the ENM-containing solution (top row) and from the porcine skin tissue injected (positive control) with the same solution (bottom row). Columns show ceria and alumina Raman shifts, respectively. The presence of ceria in both aqueous solution and skin tissue created a Raman peak at 464 cm^{-1} as seen in the red dotted triangle, while alumina created peaks at 1369 and 1399 cm^{-1} in both solution and tissue. The bottom row shows the overlay of the spectral shifts created from the skin tissue without ENMs (green) and from the skin tissue with ENMs (blue for ceria; red for alumina). [Color figure can be viewed in the online issue, which is available at wileyonlinelibrary.com.]

to produce an RSL (SL filtered against the negative tissue control sample) was justified. The possibility of creating the RSL from the ENMs suspended in an aqueous solution was explored and compared to that of the ENM-injected tissue positive control, as shown in Figure 5, where the spectral signature for the ENMs embedded in skin tissue was different from the spectral signature for the ENMs suspended in aqueous solution, creating different mapping results. This result was expected since the spectral profiles of ENMs are matrix- and microenvironment-dependent (Roth et al., 2015b).

One RSL was created for ceria and alumina, respectively, by removing the background spectra created by the skin tissue itself. Figure 1 shows the positive control samples mapped against the RSL.

Presence of ENMs in Porcine Skin Validated by RS

ENM-containing solutions used to create the positive control porcine skin samples were analyzed with RS using 532 nm for ceria and 633 nm for alumina laser beams, obtaining spectral peaks at 465 cm^{-1} for ceria, and two peaks at 1369 and 1399 cm^{-1} for alumina. The positive control skin samples were then analyzed with RS using the same respective laser beams for each element, and spectral peaks at 465 cm^{-1} in the case of ceria particles, and at 1369 and 1399 cm^{-1} for alumina particles were also obtained as expected, confirming the presence of the same particles for ceria and alumina in both the solution and skin samples (Fig. 2).

Presence of ENMs in Porcine Skin Validated by SEM-EDS

The tissue positive controls were analyzed using SEM-EDS. SEM images indicate the presence of ceria and alumina nanoparticles contouring the adipocytes in exposed subcutaneous tissue, as expected. The EDS elemental analysis also shows clear peaks of cerium and oxygen (Fig. 3) and aluminum and oxygen (Fig. 4) within the sample. Elemental mapping based on the relative abundance of elements also indicates the presence of silicon dioxide (from the glass slide on which the sample sits) and demonstrates the biodistribution

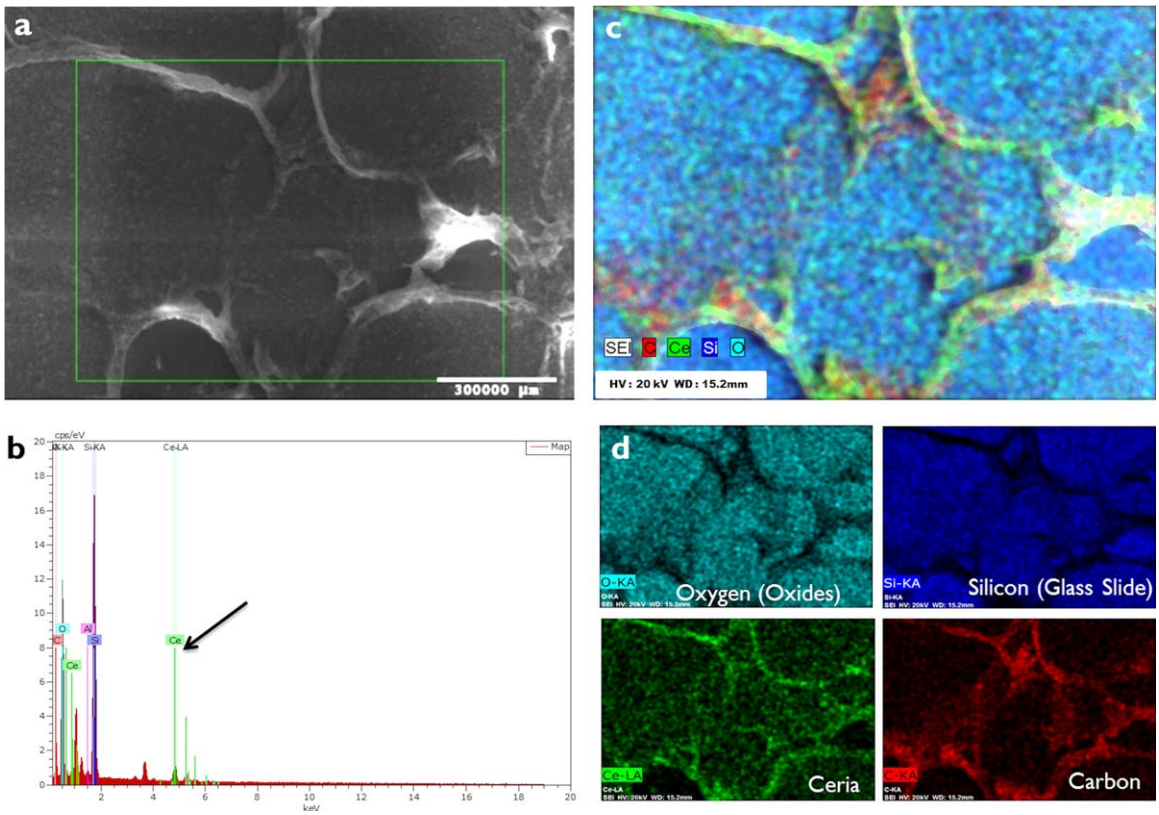

Fig. 3. SEM images indicating the presence of ceria nanoparticles in porcine subcutaneous tissue. (a) In this SEM image of a porcine tissue section, ceria nanoparticles can be seen as small specks (green) along the border of the adipocytes in the subcutaneous tissue layer. (b) The characteristic EDS peak of ceria indicated by an arrow confirms its presence in the tissue. (c) EDS elemental mapping overlay of all the elements found in the region. (d) Individual panel representing oxides in sky blue, silicon in dark blue, carbon in red, and ceria in green. [Color figure can be viewed in the online issue, which is available at wileyonlinelibrary.com.]

of ceria and alumina nanoparticles within the subcutaneous tissue.

HSI Mapping for Experimental Samples

Identification of high-contrast elements in experimental samples that were topically exposed to ENMs in solution was achieved by EDFM-HSI. Each datacube was mapped against its corresponding RSL using the SAM function, where the areas with ENMs are shown in a distinctive color, overlaid on the original datacube (Fig. 6). The images correspond to different skin layers of different porcine samples. Some high-contrast areas did not show one-to-one mapping to RSLs, which determined that not all of the high-contrast areas were occupied by the ENM of interest. The lack of one-to-one mapping in some areas shows that not everything that is high contrast in an EDFM image corresponds to the ENMs of interest, and it is particularly difficult to distinguish them from any other material with an irregular shape that may be bright under EDFM, thus the need to confirm these findings with other methods and the need to utilize EDFM always in conjunction with HSI mapping to determine the accurate location of the ENMs in the sample.

DISCUSSION

Both EDFM and HSI are effective tools for identifying high-contrast elements in porcine histological samples that have been processed for regular bright-field microscopy, and through its SAM feature, the tools are able to determine the presence of the nanoparticles of interest within the tissue. Since HSI is a relatively new technology for the detection of nanoparticles in different sample types, the confirmation of its findings with other traditional methods (RS and SEM-EDS) is necessary. Furthermore, morphologically indistinctive ENMs, such as the metal oxides in this study, could be mistaken for other components in the sample, necessitating confirmation with other methods (Husain et al., 2015). RS detected the presence of the characteristic spectral peaks for ceria (465 cm^{-1}) and alumina (1369 and 1399 cm^{-1}), as shown in Figure 2, while SEM-EDS validated the presence of ENMs in the samples, providing elemental composition and biodistribution of the nanoparticles of interest. Under RS, the same spectral peaks that were found in the EMN-containing solutions were expected to be found in the skin samples exposed to each particular solution and not to be found in nonexposed skin samples. As seen in Figure 2, the peaks found in the ENMs in aqueous solution for both ceria and alumina were found in their respective exposed skin tissue samples and were absent in

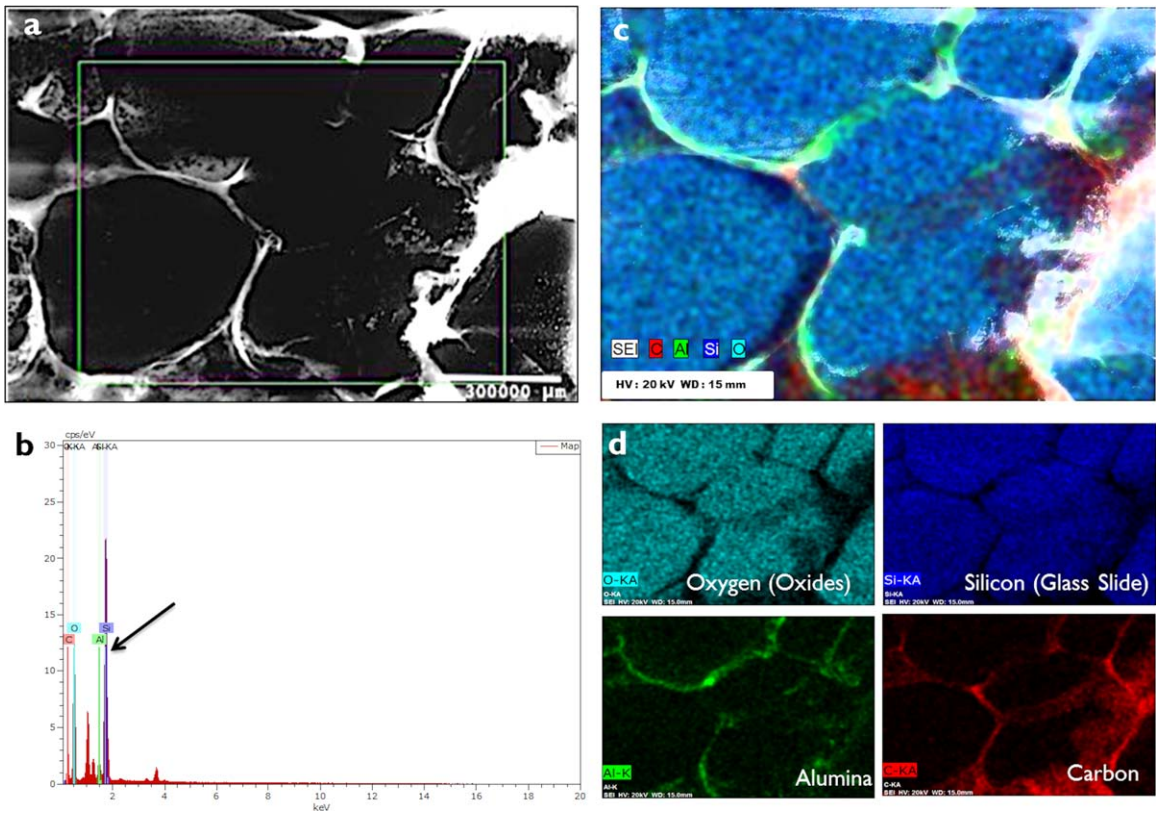

Fig. 4. SEM images indicating the presence of alumina nanoparticles in porcine subcutaneous tissue. (a) In this SEM image of a porcine tissue section, alumina nanoparticles can be seen as small specks (green) along the border of the adipocytes in the subcutaneous tissue layer. (b) The characteristic EDS peak of alumina, indicated by an arrow, confirms its presence in the tissue. (c) EDS elemental mapping overlay of all the elements found in the region. (d) Individual panel representing oxides in sky blue, silicon in dark blue, carbon in red, and alumina in green. [Color figure can be viewed in the online issue, which is available at wileyonlinelibrary.com.]

nonexposed samples. It is important to note that for the characterization of the ceria and alumina nanoparticles in the ENM-containing solution using RS, a silicon substrate was used as a platform for the sample since using a regular microscopy glass slide as a platform produced such a strong Si signal that it overpowered the signals for the ENMs of interest. This explains the difference in the peak intensity for ceria when analyzed in aqueous solution versus skin tissue. While the ceria peak was strong in the aqueous solution, its intensity decreased in the skin tissue sample although it was still perceptible. Even though the confirmation of EDFM-HSI findings with another method is required to create an accurate RSL, once this first step is accomplished, the use of the rapid HSI mapping method can then be used alone to detect and localize the ENMs of interest in a high volume of experimental biological samples.

The creation of SLs from the ENMs in different matrices is of importance as the difference in spectral profiles for the same nanoparticle could be altered by its microenvironment, as reported by Roth et al. (2015b). Even though there are reports where the raw nanoparticles were used to create an SL to map over biological samples (Husain et al., 2013, 2015), the SL utilized in this study was derived from the ENM-injected tissue positive control samples as the difference between the spectral profiles of the raw ENMs in solution versus the tissue positive control samples was evident, as shown in Figure 5. This is a key consideration in application of this technique, as the experimental design must take into account how to generate the most sensitive and specific RSL for the given research question. Additionally, HSI can be a useful tool for studying how spectral profiles for a given material change based on their microenvironment, particle size, agglomeration state, and/or surface characteristics (Shannahan et al., 2015). An in-depth investigation of the spectral data could provide more characterization information regarding the ENMs of interest. For this study, as the matrix of the positive controls was the same as the matrix of the experimental samples, the positive controls were more appropriate to use to create the RSLs. Even though the raw ENMs generated fewer unique spectra when compared to the spectral profile of the ENMs in tissue, as shown in Figure 5, it is important to consider that during the filtering process of each SL, all redundant or background spectra are removed, making the SL more efficient for mapping purposes without compromising the mapping results, and thus it cannot be responsible for the mapping differences. Further, efficient mapping may be possible with the identification of just a few unique spectra (Badireddy et al., 2012). Last, mapping may be improved with the adjustment of the SAM threshold; however, researchers must take caution in adjusting the SAM threshold

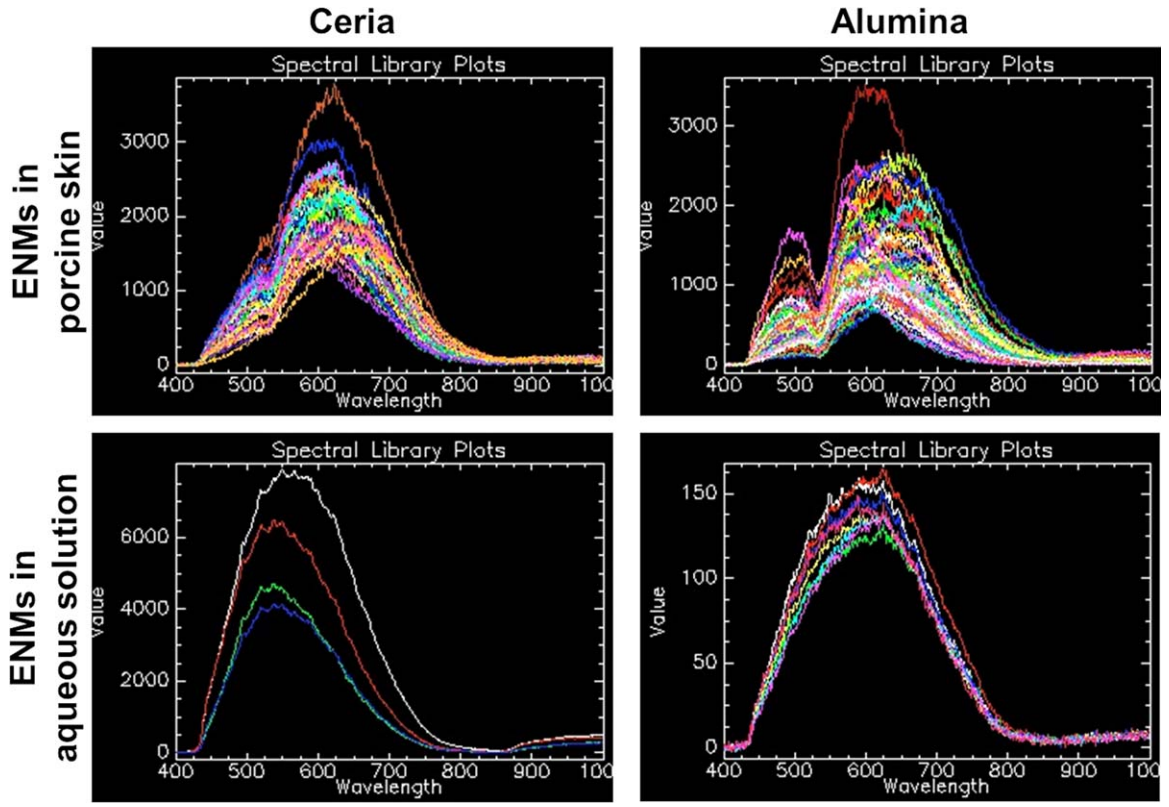

Fig. 5. HSI spectral library of metal oxide nanoparticles in porcine skin tissue compared to metal oxide nanoparticles in aqueous solution. Images correspond to the spectral profile of ceria and alumina nanoparticles, respectively (column 1 and 2). The first row corresponds to the spectral profile produced by the ENMs found in the positive controls. Bimodal peaks appear for both ceria and alumina in positive control samples, whereas the peaks for the ENMs in aqueous solution appear at different wavelengths than their tissue counterparts. The importance of this finding is that an RSL for the purpose of elemental mapping should be generated from a positive control, wherein the element of interest is contained in the same matrix as the experimental samples. [Color figure can be viewed in the online issue, which is available at wileyonlinelibrary.com.]

so that mapping remains specific to the ENMs of interest and does not incorporate false positives.

While the EDFM-HSI system offers multiple advantages over conventional methods, there are certain limitations that should be considered. For example, in this study, ENM translocation through the skin layers could be affected by the processing, preparation, and handling of the skin tissue, which could affect the results of a quantitative evaluation. HSI also has a lower spatial resolution than EM, as described by Roth et al. (2015b,c). It is also important to note that certain materials with high reflectance, such as noble metals, are more amenable to EDFM-HSI analysis, whereas other materials, such as semimetallic oxides and carbon-based nanomaterials, may prove challenging for SL creation and spectral mapping (Manolakis et al., 2003; Mercer et al., 2013b; Roth et al., 2015b).

For both RS and SEM-EDS, unstained noncoverslipped adjacent histological samples were obtained. Since these samples were not coverslipped, they remained embedded in paraffin, which was removed by a heating process and subsequent immersion in xylene. This deparaffinization process, which required drying a liquid on a solid surface, could have induced a coffee-ring effect which may have led to the deposition of nanoparticles in a ring-like manner (Yunker et al., 2011), which could affect their distribution within the sample, explaining the difference in biodistribution seen in EDFM-HSI and SEM.

Choosing an appropriate sample to serve as the basis for the creation of SLs is of great relevance when developing a protocol to achieve good, reliable, and adequate mapping results. Moreover, the creation of an accurate SL that will ensure high specificity for the identification of the ENMs of interest is highly dependent on reliable negative controls. As the SL filtering process involves the removal of redundant spectra between the positive and negative controls, the resulting reference SL could be significantly altered if contamination with the ENMs of interest was present in the negative control (Roth et al., 2015b). Finally, the HSI technique can only potentially serve as a semi-quantitative tool as no *z*-axis is available to obtain the total organ burden of a certain material.

A limitation of RS is the need for unstained, noncoverslipped adjacent tissue samples that requires an extra drying process that could alter the biodistribution of the material of interest. Also, the use of a silicon substrate for the detection of the elements of interest in the aqueous solutions was required, and the availability of these substrates may become problematic. The same unstained noncoverslipped tissue samples

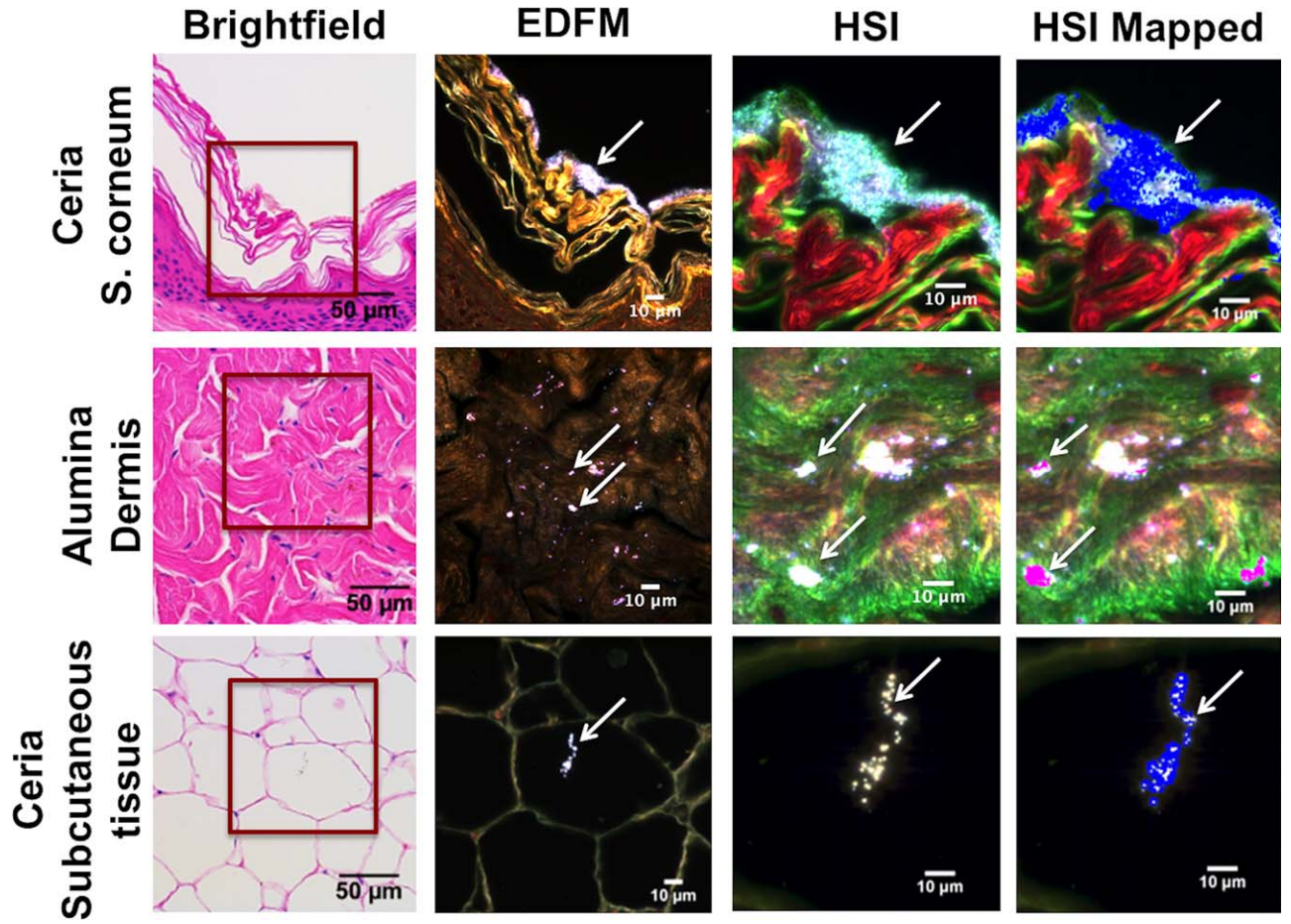

Fig. 6. Porcine skin tissue exposed to ENM-containing solution and mapped against the reference spectral library (RSL). Rows correspond to porcine skin tissue exposed to ceria and alumina ENMs, respectively (experimental samples). Each column shows the same field of view imaged with different techniques. The first column corresponds to a bright-field image of an H&E stained sample (40× magnification). The area enclosed in a red square was magnified to 100× and viewed using EDFM (column 2) and HSI (column 3), where ENMs appear as high-contrast elements (arrows). Column 4 shows the HSI image mapped against the RSL, where the positive matches are shown in blue for ceria and in magenta for alumina. From top to bottom, the rows correspond to stratum corneum, dermis, and subcutaneous tissue, respectively. [Color figure can be viewed in the online issue, which is available at wileyonlinelibrary.com.]

were required for SEM-EDS, where the biodistribution limitations and the high time and cost investments apply to these tools as well.

CONCLUSIONS

The comparison of EDFM-HSI with known methods validates the findings of this novel method for the localization and identification of ENMs in histological samples, making it an attractive alternative to more conventional techniques. This method confers several advantages over the conventional gold standard of EM in terms of time and cost reduction, despite requiring confirmation with other methods to create RSLs when analyzing indistinctively shaped ENMs. Even though precise localization of ENMs in tissue samples can be achieved with EM, its very small field of view becomes a limitation for rapid scanning. For instance, while it takes 15 min to scan a 1.5 cm × 1.5 cm skin tissue section at 10× magnification with EDFM and an additional 15 min to obtain an HSI datacube, it could take a minimum of 5 months (8 h/day, 5 days/week) to scan the same sample with TEM at "low" 1,000× magnification. Moreover, while EM must be operated by highly specialized and trained personnel, EDFM-HSI can be performed by a relatively inexperienced individual with a minimum of a few days of intensive training, not to mention the substantial difference in the cost of the instruments and potential availability of the tools in research laboratories. The significant cost differential between an EDFM-HSI system (~$155,000) and a TEM ($1–4 M) or SEM [$500,000 (entry grade) to $1M (top-of-the-line)] with EDS ($100,000) makes this an affordable in-house analysis option for research teams. Moreover, EDFM-HSI is also capable of visualizing ENMs in tissues that appear as is, without the use of a special dye or marker that other techniques require. Although not necessary for EDFM-HSI, we used H&E stain in this study to facilitate bright-field visualization, which demonstrated a much faster scanning of the sample in combination with EDFM than with regular bright-field alone.

In conclusion, this study demonstrates the utility of EDFM-HSI in identifying and localizing ENMs when

confirmed by conventional methods in fixed porcine skin tissue, which serves as a toxicological model for real-world cutaneous exposure to metal oxide ENMs associated with the semiconductor manufacturing processes. The confirmation of this method by RS and SEM-EDS supports the use of the EDFM-HSI system as a valuable tool for this purpose, providing multiple advantages over traditional EM or RS techniques, including faster acquisition time, reduced costs, and tissue structure preservation. Moreover, due to the multiple analysis tools in the HSI software, a further semiquantitative analysis of ENMs could be possible. This paves the way not only for its use in further analysis, such as investigating the penetration and semiquantitation of ENMs through layers of skin tissue, but also for efficient analysis of other nanoparticles in biological samples. This technique may be an attractive option for investigators who require rapid results, lack the expertise in conducting EM themselves, and/or lack the necessary funds for extensive, high-throughput commercial EM analysis of samples.

ACKNOWLEDGMENTS

The authors thank the Albert Einstein College of Medicine Histology and Comparative Pathology Facility (Rani Sellers, DVM, PhD; Barbara Cannella, PhD); Bushra Alam, PhD for technical assistance with EM and RS; Gary Roth, PhD for technical assistance with HSI; Kathleen Dunn, PhD for manuscript review; and Elyse Johnson for technical support with HSI.

REFERENCES

Badireddy AR, Wiesner MR, Liu J. 2012. Detection, characterization, and abundance of engineered nanoparticles in complex waters by hyperspectral imagery with enhanced darkfield microscopy. Environ Sci Technol 46:10081–10088.

Brenner SA, Neu-Baker NM, Caglayan C, Zurbenko IG. 2015. Occupational exposure to airborne nanomaterials: An assessment of worker exposure to aerosolized metal oxide nanoparticles in semiconductor wastewater treatment. J Occup Environ Hyg 12:469–481. doi:10.1080/15459624.2015.1018515.

Brenner SA, Neu-Baker NM. 2015. Occupational exposure to nanomaterials: Assessing the potential for cutaneous exposure to metal oxide nanoparticles in a semiconductor facility. J Chem Health Safety 22:10–19. doi:10.1016/j.jchas.2014.11.001.

Edwards HGM. 2005. Modern Raman spectroscopy—A practical approach. Chichester, UK: John Wiley and Sons. p.210.

Husain M, Saber AT, Guo C, Jacobsen NR, Jensen KA, Yauk CL, Williams A, Vogel U, Wallin H, Halappanavar S. 2013. Pulmonary instillation of low doses of titanium dioxide nanoparticles in mice leads to particle retention and gene expression changes in the absence of inflammation. Toxicol Appl Pharmacol 269-3:250–262.

Husain M, Wu D, Saber AT, Decan N, Jacobsen NR, Williams A, Yauk CL, Wallin H, Vogel U, Halappanavar S. 2015. Intratracheally instilled titanium dioxide nanoparticles translocate to heart and liver and activate complement cascade in the heart of C57BL/6 mice. Nanotoxicology 20:1–10.

Ilves M, Palomaki J, Vippola M, Lehto M, Savolainen K, Savinko T, Alenius H. 2014. Topically applied ZnO nanoparticles suppress allergen induced skin inflammation but induce vigorous IgE production in the atopic dermatitis mouse model. Part. Fibre Toxicol 11:38

Jestel NL. 2010. Raman spectroscopy, in process analytical technology: Spectroscopic tools and implementation strategies for the chemical and pharmaceutical industries. Chichester, UK: John Wiley & Sons.

Kumar GL, Kiernan JA. (Eds.) 2010. Special stains and H&E. Carpinteria, California: Dako North America.

Kwok KWH, Auffan M, Badireddy AR, Nelson CM, Wiesner MR, Chilkoti A, Liu J, Marinakos SM, Hinton DE. 2012. Uptake of silver nanoparticles and toxicity to early life stages of Japanese medaka (*Oryzias latipes)*: Effect of coating materials. Aquatic Toxicol 120-121:59–66.

Ma JY, Mercer RR, Barger M, Schwegler-Berry D, Scabilloni J, Ma JK, Castranova V. 2012. Induction of pulmonary fibrosis by cerium oxide nanoparticles. Toxicol Appl Pharmacol 262:255–264.

Manolakis D, Marden D, Shaw GA. 2003. Hyperspectral image processing for automatic target detection applications. Lincoln Lab J 14:79–116.

Mercer RR, Scabilloni JF, Hubbs AF, Battelli LA, McKinney W, Friend S, Wolfarth MG, Andrew M, Castranova V, Porter DW. 2013. Distribution and fibrotic response following inhalation exposure to multi-walled carbon nanotubes. Part Fibre Toxicol 10:33

Mercer RR, Scabilloni JF, Hubbs AF, Wang L, Battelli LA, McKinney W, Castranova V, Porter DW. 2013b. Extrapulmonary transport of MWCNT following inhalation exposure. Part Fibre Toxicol 10:38

Roco MC, Mirkin CA, Hersam MC. 2010. WTEC panel report on nanotechnology research directions for societal needs in 2020: retrospective and outlook. WTEC.

Roth GA, Neu-Baker NM, Brenner SA. 2015a. SEM analysis of particle size during conventional treatment of CMP process wastewater. Sci Tot Environ 508:1–6. doi:10.1016/j.scitotenv.2014.11.075.

Roth GA, Sosa Peña MP, Neu-Baker NM, Tahiliani S, Brenner SA. 2015b. Identification of metal oxide nanoparticles in histological samples by enhanced darkfield microscopy and hyperspectral mapping. J Vis Exp 106:53317. doi:10.3791/53317.

Roth GA, Tahiliani S, Neu-Baker NM, Tahiliani S, Brenner SA. 2015c. Hyperspectral microscopy as an analytical tool for nanomaterials. WIREs Nanomed Nanobiotechnol 7:565–579. doi:10.1002/wnan.1330.

Roth GA, Neu-Baker NM, Brenner SA. 2015d. Comparative characterization methods for metal oxide nanoparticles in aqueous suspensions. J Chem Health Safety 22:26–32. doi:10.1016/j.jchas.2015.02.001.

Shannahan JH, Podila R, Brown JM. 2015. A hyperspectral and toxicological analysis of protein corona impact on silver nanoparticle properties, intracellular modifications, and macrophage activation. Int J Nanomed 10:6509–6521.

Shepard MN, Brenner S. 2014a. An occupational exposure assessment for engineered nanoparticles used in semiconductor fabrication. Ann Occup Hyg 58:251–265. doi: 10.1093/annhyg/met064.

Shepard M, Brenner S. 2014b. Cutaneous exposure scenarios for engineered nanoparticles used in semiconductor fabrication: A preliminary investigation of workplace surface contamination. Int J Occup Environ Health 20:247–257. doi: 10.1179/2049396714Y.0000000074.

Titford M. 2009. Progress in the development of microscopical techniques for diagnostic pathology. J Histotechnol 32:9–19.

Vetten MA, Tlotleng N, Tanner Rascher D, Skepu A, Keter FK, Boodhia K, Koekemoer LA, Andraos C, Tshikhudo R, Gulumian M. 2013. Label-free in vitro toxicity and uptake assessment of citrate stabilised gold nanoparticles in three cell lines. Part Fibre Toxicol 10:50

Yunker PJ, Still T, Lohr MA, Yodh AG. 2011. Suppression of the coffee-ring effect by shape-dependent capillary interactions. Nature 476:308–311.

Zheng J, Nagashima K, Parmiter D, de la Cruz J, Patri AK. 2011. SEM X-ray microanalysis of nanoparticles present in tissue or cultured cell thin sections. In Characterization of nanoparticles intended for drug delivery, Humana Press. p. 93–99.